Molecular mechanism of complement inhibition by the trypanosome receptor ISG65

Alexander D. Cook[1,2], Mark Carrington[3,*] and Matthew K. Higgins[1,2,*]

[1] Department of Biochemistry, University of Oxford, South Parks Road, Oxford OX1 3QU, UK.

[2] Kavli Institute for Nanoscience Discovery, Dorothy Crowfoot Hodgkin Building, University of Oxford, South Parks Rd, Oxford, OX1 3QU

[3] Department of Biochemistry, University of Cambridge, Tennis Court Road, Cambridge CB2 1QW, UK.

*Corresponding authors: matthew.higgins@bioch.ox.ac.uk and mc115@cam.ac.uk

Abstract

African trypanosomes replicate within infected mammals where they are constantly exposed to the molecules of the complement system. This system centres around complement factor C3, which is present in a soluble form in serum but can become covalently deposited onto the surfaces of pathogens after proteolytic cleavage to C3b. Membrane-associated C3b triggers different complement-mediated effectors which promote pathogen clearance, including complement receptor-mediated stimulation of immune cells or recruitment of components of the pore-forming membrane attack complex. To counter complement-mediated clearance, African trypanosomes have a cell surface receptor, ISG65, which binds to C3b and which decreases the rate of trypanosome clearance in an infection model. However, the mechanism by which ISG65 reduces C3b function had not been determined. We reveal through cryogenic electron microscopy that ISG65 has two distinct binding sites for C3b, only one of which is available in C3, ensuring that ISG65 preferentially binds to active C3b. We show that ISG65 does not block the formation of C3b or the function of the C3 convertase which catalyses the surface deposition of C3b. However, we show that ISG65 forms a specific conjugate with C3b, perhaps acting as a decoy. ISG65 also occludes the binding sites for complement receptors 2 and 3, which will disrupt recruitment of immune cells, including B cells, phagocytes and granulocytes. This suggests that ISG65 protects trypanosomes by combining multiple approaches to dampen the complement cascade.

Introduction

African trypanosomes can survive in the blood and tissue spaces of mammals for decades[1], despite constant exposure to the molecules and cells of the immune system. They have evolved a unique surface coat packed with many copies of a single variant surface glycoprotein (VSG)[2]. At a population level, antigenically distinct VSGs are expressed over the course of an infection, thereby preventing antibody-mediated clearance[3]. In addition to the need to resist acquired immunity, trypanosomes must also evade innate immune processes, such as the complement system. Recent studies have identified receptors which function within the trypanosome surface coat and which bind to either complement factor C3b[4] or complement modulator factor H[5]. ISG65 was identified as the trypanosome C3b receptor and has been shown to reduce the susceptibility of trypanosomes to antibody-mediated clearance in a mouse infection model[4]. However, we have little insight into the molecular mechanisms underpinning complement resistance mediated by ISG65.

The complement system involves a complex set of molecular cascades[6,7]. These converge at the conversion of serum complement C3 into C3b and the deposition of C3b on a pathogen surface through the formation of a thioester bond between the TED domain of C3b and cell surface components[8]. C3b deposition can occur through three major and distinct pathways. In the classical pathway, antibodies mediate recruitment of C3b, while in the lectin pathway, this results from recognition of cell surface glycans. In both cases, these events establish C4bC2b convertases, which catalyse the conversion of C3 into C3b and its surface deposition. In contrast, the alternative pathway involves stochastic conversion of C3 into C3b, resulting in an initial deposition event independent of other molecular recognition processes[9]. The first deposited C3b molecules can then assemble with factors B and D, leading to formation of the C3 convertase, C3bBb, which catalyses deposition of further C3b molecules and amplification of downstream responses[10].

The outcomes of C3b deposition are also diverse, involving both the cellular and molecular branches of the immune system. Direct recognition of immobilised C3b, or its cleavage products iC3b, C3dg, and C3d, by complement receptors stimulates the activity of various immune cells. Complement receptor 1 (CR1) is found on macrophages and binding of CR1 to C3b promotes phagocytosis of pathogens such as *Leishmania*[11]. Complement receptor 2 (CR2) is found on B cells and forms a signal transducing B cell co-receptor with CD19 and CD81[12]. CR2-CD19-CD81 is stimulated upon binding to C3d, and the absence of CR2 severely attenuates humoral immunity[13,14]. Complement receptors 3 and 4 are integrins

found on various leukocytes and are associated with diverse effects, such as enhancement of natural killer cell cytotoxicity and antibody-dependent eosinophil cytotoxicity against schistosomes[15,16]. Through mechanisms distinct from those mediated by complement receptors, C3b can trigger a cascade which leads to recruitment of the pore-forming membrane attack complex[17]. Here, deposited C3b binds to other complement factors, resulting in formation of a C5 convertase. This cleaves complement factor C5, generating C5b, which becomes membrane associated. C5b triggers the recruitment of factors C6-9 to the pathogen surface, leading to the formation of a pore which mediates cell death[18].

Pathogens have evolved a wide range of different approaches to evade complement-mediated destruction by regulating different stages of the complement cascade[7,19]. These include *S. aureus* Efb-C which binds to the TED domain of C3 and prevents the conformational change required to generate C3b[20]; *S. aureus* Efb, Ehp and Sbi which bind to the TED domain of C3/C3d and prevent binding of complement receptor 2, thereby inhibiting B cell recruitment[21,22]; smallpox virus SPICE which displaces factor B, preventing C3 convertase function[23]; and *S. aureus* SCIN and Sbi which bind to the C3bBb C3 convertase and hold it in an inactive conformation[24,25]. This therefore raised the question of how ISG65 regulates complement mediated processes. Does it inhibit the deposition of C3b by preventing the function of C3 convertases? Does it block the recognition of C3b by complement receptors, thereby reducing recruitment of immune cells? Does it block the function of the C5 convertase, preventing the formation of the membrane attack complex? Here, we combine structural biology and biophysical methods to show that ISG65 does not block C3 convertase formation, but instead combines multiple functionalities to dampen the outcomes of C3b deposition.

Results

Two distinct binding sites connect C3b to ISG65

We previously determined the crystal structure of ISG65 bound to C3d (equivalent to the TED domain of C3b), revealing how the three core helices of ISG65 form a concave surface to which C3d binds[4]. However, this study also showed that this structure does not reveal the full interaction interface between ISG65 and C3b. Surface plasmon resonance had been used to measure the affinities of ISG65 for different domains of C3, with dissociation constants of 602nM for C3d (the TED domain) and 40nM for C3b[4]. This suggested that ISG65 forms contacts with C3b in addition to those structurally characterised with the TED domain.

To provide a full molecular model of ISG65 bound to C3b we used cryogenic electron microscopy (Figure 1). We prepared ISG65-C3b complex in the presence of fluorinated octyl maltoside, which improved particle distribution in grids while avoiding dissociation of the complex. We collected 14,339 movies from which particles were extracted and a three-dimensional volume was calculated. To improve the resolution of the region containing the binding site, local refinement was performed using a mask covering ISG65 and the TED and CUB domains of C3b, resulting in a volume at 3.4 Å resolution. Guided by previous structures of ISG65[4] and C3b[26] and by an Alphafold2[27] model of ISG65, we were able to build a molecular model for the ISG65-C3b complex (Figure 1, Supplementary Figure 1, Supplementary Table 1).

This structure reveals the two distinct interfaces formed between ISG65 and C3b (Figure 2a). The first of these, interface 1, matches that previously identified through our crystallographic analysis[4], with no significant differences between the models in this region. However, whilst our previous structure did not have interpretable electron density for loops L2 and L3, perhaps due to their disorder, or due to proteolytic damage during crystallisation. However, these loops were resolved in our cryogenic electron microscopy-derived volume. This allowed us to build a *de novo* model for residues 155-195 and 230-250. In particular, loop 2 forms a direct contact with the CUB domain of ISG65, centred around an electrostatic

interaction mediated by C3b residue Arg954. The presence of this additional contact between ISG65 and C3b, which is not present between ISG65 and the TED domain alone, explains the difference in affinity between these interactions.

The conversion of C3 to C3b is accompanied by a substantial conformational change, which involves a large movement of the TED domain. If we dock ISG65 onto the structure of C3[28] using interface 1, then interface 2 cannot form (Figure 2b). To check the effect of the lack of this interaction interface on affinity, we used surface plasmon resonance analysis to measure the binding of human serum, C3 and C3b to immobilised ISG65 (Figure 2c, Supplementary Table 2). We previously observed that the binding of C3b to ISG65 fitted to a two-state binding model, with an affinity of 40nM[4]. In contrast, we now observed that C3 binding to ISG65 fitted to a one site binding model, with an affinity of 240nM. This was confirmed by the binding responses when serum was flowed over ISG65. The responses revealed on- and off-rates which closely matched those for C3, as expected due to the predominance of C3 over C3b in serum. The formation of two interfaces between ISG65 and C3b, of which only one can occur with C3, will lead to preferential binding of C3b to ISG65, allowing ISG65 to favour modulation of the activity of surface bound C3b, while limiting any role in the binding of serum C3 on the trypanosome surface.

ISG65 does not inhibit the formation of the C3 convertase but does form a specific covalent conjugate with C3b

In addition to determining the structure of C3b bound to ISG65, the same data set also yielded a three-dimensional class consisting of a structure of unbound C3b. This allowed us to discover whether the presence of ISG65 caused a conformational change in C3b (Figure 3a). Fitting the model of the C3b-ISG65 complex into the volume derived for the complex resulted in a map-model correlation of 0.76. When we fitted the same model into the volume derived from C3b alone, the correlation was 0.73, indicating that the ISG65-bound conformation of C3b is equivalent to the free conformation of C3b. Therefore, unlike bacterial C3b-effector proteins, such as Efb-C[20], ISG65 does not prevent C3 from adopting the active conformation of C3b. Indeed, this is consistent with ISG65 binding to C3b already conjugated to the trypanosome surface, rather than preventing C3b formation.

The initial conjugation of C3b to the trypanosome surface is followed by formation of the C3 convertase, consisting of C3b bound to factor Bb (C3bBb). This requires factor B to first bind to C3b and then be cleaved by factor D to generate C3bBb. In order to determine whether ISG65 can block C3bBb formation, we first compared the ISG65-C3b structure with those of C3b bound to factors B and D[29]. We found that ISG65 does not complete with either factor B or Factor D and does not block the binding of factor Bb (Figure 3b). This suggests that the C3 convertase can form in the presence of ISG65.

We next developed an *in vitro* assay for C3 convertase formation in which we combined C3 and factor B with catalytic quantities of C3b and factor D. When mixed *in vitro*, this triggered the cleavage of C3 to C3b, as shown by the production of C3a. In addition, it resulted in the cleavage of factor B to form Bb and Ba (Figure 3c). When performed in a >3-fold excess of ISG65, the production of C3a and Ba were unaltered, indicating that formation of the C3bBb C3 convertase can proceed in the presence of ISG65. (Figure 3c).

Comparison of the outcome of C3 convertase formation in the presence and absence of ISG65, revealed that in the presence of ISG65 a high molecular weight band appeared, which we identified through mass spectrometry to be a conjugate of ISG65 with C3b (Figure 3c). When we conducted the equivalent experiment, using the same amount of bovine serum albumin instead of ISG65, we did not observe the formation of this conjugate, suggesting that it occurs specifically due to the proximity of ISG65 and the thioester-forming residue of C3b when in the complex (Figure 3d). Finally, to identify which region of ISG65 is responsible for the formation of this conjugate, we used versions of ISG65 which lack loops L1, L2 or L3, or which lacked the flexible C-terminal region. In each of the loop mutants, we

still observed the formation of the ISG65-C3b conjugate. However, this was not observed in the ΔC mutant (Figure 3e). This C-terminal region is an unstructured string of 72 amino acids that does not form part of the binding site for C3b and is not observed in the structures. It forms a flexible linker which connects the structured ISG65 domain to the plasma membrane. These data therefore suggest that the proximity of the flexible linker of ISG65 to the thioester site of C3b leads to the formation of a preferential conjugate between ISG65 and C3b, perhaps acting as a decoy to reduce the conjugation of C3b to other regions of the trypanosome surface.

ISG65 blocks the binding of complement receptor 2 and 3 to C3b and C3d

As the central component of the complement system, C3 is the target of many host-proteins[8]. These factors can be broadly grouped into the complement receptors, which are found on immune cells and bind to C3b, iC3b, C3db, and C3d fragments, and factors that regulate the activity of C3b. Complement regulators typically act by blocking recognition of C3b by host-factors to prevent down-stream activation[30]. To test whether ISG65 might influence the capacity of complement regulators and receptors to bind to C3b/d, we next compared the structure of ISG65-bound C3b with previously determined structures of C3b and C3d bound to such proteins (Figure 4).

The conformation and location of ISG65 bound to C3d demonstrated that ISG65 binding would preclude binding of Factor H domains 19-20[31]. However, the impact of ISG65 on the binding of complement receptors to C3b is variable. The binding site on C3b for ISG65 does not overlap with those for C3b-binding complement receptors CRIg[32] and complement receptor 1 (CR1)[33]. However, the region on C3d occupied by ISG65 overlaps with sites on the TED domain/C3d which bind complement receptors 2 (CR2)[34] and 3 (CR3)[35] (Figure 4). CR2 is a receptor found on B cells, which in complex with CD19 and CD81, forms a signal transducing B-cell co-receptor[12]. Binding of C3d to CR2 greatly reduces the threshold for B cell activation, thereby triggering B cell activation and antibody production[14]. By inhibiting binding of CR2 to C3d, ISG65 will reduce the likelihood that B-cell receptor binding to trypanosome antigens will result in B-cell activation and antibody production. Similarly, the binding site of CR3 on C3d also overlaps with that for ISG65, suggesting that ISG65 will block CR3 binding. CR3 is widely expressed on various immune cells and is known to promote macrophage recruitment and phagocytosis by binding to iC3b/C3d, indicating that ISG65 may help reduce trypanosome clearance by blocking this interaction[15].

Discussion

The long-term survival of a pathogen in a mammalian host can only occur if it has evolved strategies to avoid clearance by all arms of the host immune system, including the complement system. In a previous study we highlighted the importance of the complement system in the clearance of trypanosomes during the first wave of infection in a mammalian infection model[4]. Mice infected with trypanosomes showed two waves of infection. The first peaked around five days after infection and was partially controlled. Around eight days after infection, a second wave was initiated, most likely due to trypanosomes which had undergone antigenic variation through switching their VSG coat. When a similar infection experiment was conducted using the same trypanosome cell line to infect mice lacking complement C3, then the first wave of infection was no longer controlled. This suggested that the control of the first wave of infection was mediated by both antibodies and by complement, implicating the classical complement pathway. When wild-type mice were infected with trypanosomes lacking the complement C3/C3b receptor, ISG65, the control of the first wave of infection was delayed, suggesting that ISG65 reduces the susceptibility of trypanosomes to destruction by complement[4]. However, this study did not investigate the molecular mechanism by which ISG65 reduces the activity of complement.

Our previous structural studies revealed that ISG65 binds to C3d, which is equivalent to the isolated TED domain of C3b[4]. However, they also suggested that this does not describe the

full interaction interface between ISG65 and C3b, with ISG65 showing a ~10-fold higher affinity for C3b than it shows for C3d[4].To understand the molecular mechanism for ISG65 function, we therefore needed to reveal the full C3b binding mode of ISG65. We now show, through cryogenic electron microscopy, that in addition to interacting with the TED domain, ISG65 also interacts with the CUB domain of C3b, simultaneously bridging these two sites. This complete model of the ISG65-C3b complex now allows us to answer a series of questions about how ISG65 might modulate C3b function, showing whether ISG65 prevents the formation of C3b, whether it blocks formation of the C3 convertase and whether it blocks the binding of complement regulators and complement receptors to C3b.

Our first conclusion is that ISG65 will bind preferentially to C3b rather than C3. While modelling reveals that the TED domain is correctly arranged in C3 to allow ISG65 binding, the different relative organisation of the TED and CUB domains will not allow ISG65 to simultaneously interact with both domains in C3. Indeed, we find that ISG65 has an affinity >5-fold lower for C3 than it has for C3b. Indeed, in the context of a trypanosome, this difference in binding will be further amplified as C3 is monomeric in solution, while both ISG65 and C3b will be associated with the trypanosome membrane, thereby increasing their relative local concentrations. The serum concentration of C3 is 5mM and so the ~250nM affinity of ISG65 for C3 will ensure that this interaction can occur under physiological concentrations. However, the ability of ISG65 to preferentially bind, through a higher affinity interaction and through avidity, to cell surface bound C3b rather than to C3 in solution, will ensure that it partitions onto the dangerous cell-associated C3b in preference to the soluble C3 which does not threaten the trypanosome.

A second conclusion is that ISG65 does not prevent the conformational changes which occur as C3 is converted to C3b, with no difference in conformation of free C3b and ISG65-bound C3b. Neither does ISG65 prevent the formation of the C3 convertase, C3bBb. This convertase forms when C3b recruits factors B and D, leading to cleavage of factor B to generate fragments Ba and Bb, with Bb remaining bound to C3b[6]. The C3bBb convertase can then induce the formation of more C3b from C3, thereby increasing the quantity of surface bound C3b and amplifying the complement cascade. ISG65 does not block the binding sites occupied by factors B or D, or the site proposed to be occupied by subsequent C3 molecules[10]. Indeed, in a solution assay to measure C3 convertase function, we see that the presence of ISG65 has no effect on C3bBb activity.

Intriguingly, while ISG65 does not affect C3 convertase function in this solution assay, we find that a newly formed conjugate is established between the flexible C-terminal tail of ISG65 and newly formed C3b. Indeed, the location of the C-terminal tail places it close to the thioester forming residue in the context of the ISG65-C3b complex. This conjugate is not formed when BSA is included in the assay at a similar concentration, or when ISG65 lacking the C-terminal tail is used. Could the formation of this conjugate help to protect the trypanosome from the downstream effects of C3b deposition on the cell surface? The amplification of C3b deposition, and the subsequent formation of the C5 convertase, requires C3b molecules, and their binding partners, to come into close proximity. It is possible that conjugating C3b to ISG65, which will swing above the trypanosome surface on a flexible linker, might make the C3b molecules less likely to come together productively than if they were linked to sites in the VSG surface.

Finally, our complete ISG65-C3b structure shows which binding sites for other complement receptors and regulators are occluded by the presence of ISG65. Indeed, we find that the binding sites on C3b and C3d for both complement receptors 2 and 3 overlap with that of ISG65. These receptors are found on B cells and leukocytes respectively. By blocking CR2 binding, ISG65 is likely to reduce B cell activation and antibody production, while blocking CR3 binding is likely to reduce trypanosome clearance by phagocytosis and complement-mediated cytotoxicity.

Therefore, our studies show that ISG65 will dampen the outcomes of the complement system through a diverse combination of mechanisms. By enhancing its affinity for C3b through a two-site binding mechanism, ISG65 will preferentially partition onto cell surface conjugated C3b. When it binds to C3 or C3b which is approaching the cell surface, it will selectively form a conjugate between its C-terminal tail and C3b, ensuring that C3b is flexibly attached rather than more rigidly associated with VSG, perhaps altering the likelihood of it forming productive complexes, such as C5 convertases. Finally, ISG65 may block recruitment and stimulation of immune cells by the trypanosome surface, by preventing binding of CR2 and CR3. Each of these effects will contribute to dampening of the complement response, while rapid clearance of surface attached C3b through hydrodynamic forces resulting from trypanosome swimming, coupled with rapid endocytosis, cleans the trypanosome surface. Through this combination of mechanisms, the likelihood of immune activation and parasite death due to complement will decrease and the time required for the mammalian host to control the first wave of infection will be prolonged, enhancing the likelihood of transmission of the trypanosome through a tsetse fly bloodmeal.

Methods

Mammalian expression and purification of ISG65 and complement proteins

To express ISG65 1125G[4] (residues 24-385), we used a pDest12 plasmid consisting of an N-terminal secretion signal, codon optimized ISG65, a C-terminal flexible linker (GSGSGSASG), AviTag, and a His_{10}-tag. Human Complement Factor B (residues 26-764) and Complement Factor D (residues 20-253) were cloned into a pHLsec plasmid containing an N-terminal secretion signal and a short C-terminal linker (GSG) followed by a C-tag. ISG65, Factor B, and Factor D DNA were transfected into HEK293F cells (3 μg DNA per mL of cells) grown in F17 Freestyle media to a density of 2.2×10^6 cells/mL, using polyethylenimine (9 ug per mL of cells). Media was supplemented with 1 μM kifunensine and 3.8 mM valproic acid. Cell culture supernatant was harvested 6 days after transfection. Initial purification of ISG65 was performed using Ni Sepharose excel resin (Cytiva), whilst CaptureSelect C-tagXL Affinity Matrix (ThermoFisher) was used to purify Factor B and D. ISG65 and Factor D were further purified on a Superdex 75 300/10 GL (Cytiva), whilst Factor B was further purified with a Superdex 200 300/10 GL (Cytiva). ISG65 loops deletions (loop1: ΔP88-K92insSS, loop2: ΔQ155-R195, loop3: ΔK230-P250, tail: ΔK317-G394) were generated using Gibson Assembly (NEB) and expressed and purified as described for ISG65 24-385 above.

Purification of Human Complement C3 and generation of C3b

To purify Complement C3, anonymous donor post-clot human serum was obtained from the NHS Blood and Transplant non-clinical issue supply. Serum was buffer exchanged into 20 mM Tris pH 8, 50 mM NaCl, 0.5 mM EDTA using tangential flow filtration with a stack of three 100 kDa Omega Cassettes (PALL Corporation). Serum was clarified by ultra-centrifugation at 41,000 rpm in a Ti-45 rotor (Beckman-coulter). Purification of C3 was performed by anion exchange chromatography using a HiPrep Q HP 16/60 column (Cytiva) with a 20 column volume gradient of 50 to 350 mM NaCl. Fractions containing C3 were pooled then buffer exchanged into 20 mM MES pH 6, 50 mM NaCl, 0.5 mM EDTA using tangential flow filtration as above. C3 was then purified by cation exchange using a monoS 4.6/100 PE (Cytiva) with a 30 column volume gradient to 500 mM NaCl. Fractions containing C3 were then further purified on a Superdex 200 300/10 GL.

C3b was generated from C3 by limited proteolysis with trypsin (Roche) at 1 % w/w trypsin to C3 at 37°C for 2 minutes. Trypsin was then inhibited with soybean trypsin inhibitor (Merck) at a ratio of 1 % w/w inhibitor to C3.

Preparation of ISG65-C3b complexes for cryo-EM

To form C3b-ISG65 complexes, C3b was mixed with ISG65 at 1:1.1 ratio in 20 mM HEPES pH 7.4, 150 mM NaCl, 0.5 mM EDTA. Complexes were then purified on a Superdex 200 300/10 GL column. Quantifoil grids consisting of a 1.2/1.3 μm holey carbon film on 300 gold mesh were glow discharged at 15 mA for 1 minute with an EM ACE200 glow discharger (Leica). Just before vitrification, 0.01 % fluorinated octyl maltoside (Anatrace) was added to 2.2 mg/mL C3b-ISG65, which was then immediately added to the grid and plunge frozen in an ethane slush using a Vitrobot Mark IV (ThermoFisher). Grids were imaged with a Titan Krios G2 (ThermoFisher) operating at 300 kV, and images were recorded with a K3 detector (Gatan) in counting mode with a GIF Quantum LS Imaging Filter (Gatan).

Image processing and modelling of ISG65-C3b complexes.

Movies were motion corrected, contrast transfer function (CTF) corrected, and particles were picked using SIMPLE v3[36] on the fly. To obtain an initial set of C3b/C3b-ISG65 particles, one round of 2D classification was performed in SIMPLE, followed by another two rounds of 2D classification in CryoSPARC v3[37]. A second set of particles was obtained by particle picking with TOPAZ v0.2.4[38] followed by one round of 2D classification to remove bad particles. TOPAZ and SIMPLE particles were combined, duplicates removed, and a final round of 2D classification was performed. Three rounds of *ab initio* and heterogeneous 3D refinement were performed in CryoSPARC using 5 classes which resulted in a set of C3b-ISG65 particles, and a set of C3b only particles. Both particle sets were merged and yielded a 3.5 Å map from homogenous refinement in CryoSPARC. Bayesian polishing was then performed in Relion v3.1[39,40], followed by per particle CTF refinement and beam tilt estimation in CryoSPARC, yielding a 3.3 Å map. Particles were separated into C3b-ISG65 and C3b only sets, yielding 3.3 and 3.4 Å resolution maps respectively. The resolution of CUB, TED and ISG65 were significantly lower than the rest of the map presumably because of flexibility in CUB and TED, and because of the location of ISG65 on the periphery of the map. To mitigate this, particle coordinates were shifted such that CUB-TED-ISG65 density was in the middle of the box, then all density other than CUB-TED-ISG65 was subtracted using a 10-pixel soft edge mask. Local refinement was then performed using a pose/shift gaussian prior with a standard deviation of 3° over rotations and 2 Å over shifts, and search limitations of 12° and 9 Å, resulting in a 3.4 Å map. Local refinement was also performed for all density except CUB-C3d-ISG65 using a 15-pixel soft edge mask, yielding a 3.2 Å map. Post-processing was then performed using DeepEMhancer, and local resolution was estimated with CryoSPARC, and locally refined maps were combined in ChimeraX[41] to create a composite map.

To generate a model of ISG65-C3b, a previous crystal structure of C3b (PDB ID: 5FO7)[33] and a structure prediction of ISG65 performed with AlphaFold2[27] were rigid-body fitted into cryo-EM density using the fit in map tool in ChimeraX[41]. Refinement of C3b-ISG65 was then performed using ISOLDE v1.0[42] and COOT v0.9.8.3[43].

Surface plasmon resonance

SPR experiments were performed on a BIAcore T200 (Cytiva). ISG65 was biotinylated via an N-terminal Avi-tag and immobilised on the chip via streptavidin using a CAPture kit (Cytiva). C3 was run from 625 nM in 2-fold dilutions to 1.2 nM, and human serum was run from 8 mg/mL in 2-fold dilutions to 0.06 mg/mL. Measurements were performed at 30 μL/min at 25°C in 20 mM HEPES pH7.4, 300 mM NaCl, 0.05 % TWEEN-20, with an association and dissociation time of 120 s. Binding responses were obtained using BIAevalutation software v1.0, followed by fitting to a 1:1 Langmuir model.

C3 convertase activity assays

To measure the effect of ISG65 on C3 convertase activity, 600 nM C3, 600 nM Factor B, 12 nM C3b, 12 nM Factor D, and 2 μM ISG65 or 2 μM bovine serum albumin (Sigma) were combined in phosphate buffered saline pH 7.4, 2 mM $MgCl_2$. The reaction was carried out at 22°C and samples were removed at various intervals and combined with SDS-PAGE sample buffer before running on SDS-PAGE to assess band shifts in C3 and Factor B. Gel densitometry was performed in Fiji[44].

Data availability statement

Cryo-EM maps are available from the Electron Microscopy Data Bank under accession codes EMDB-17209 (C3b-ISG65 composite map), EMDB-17219 (locally aligned CUB-TED-ISG65), EMDB-17220 (locally aligned C3c region) and EMDB-17221 (C3b only), while coordinates for C3b-ISG65 are available from the Protein Data Bank under accession code 8OVB.

Acknowledgements

This work was funded through a Wellcome Investigator award (217138/Z/19/Z). We thank Olivia MacLeod for discussions about the complement system and its regulation and Rishi Matadeen, Joseph Caesar and Teige Matthews-Palmer at the COSMIC cryo-EM facility (University of Oxford) for support with data collection and data processing.

Author contributions

A.C. expressed and purified proteins, performed structure determination, C3 convertase assays and surface plasmon resonance analysis. A.C., M.C. and M.K.H. designed experiments and prepared the manuscript. M.C. and M.K.H. contributed expertise and funding.

References:

1 Sudarshi, D. *et al.* Human African Trypanosomiasis Presenting at Least 29 Years after Infection-What Can This Teach Us about the Pathogenesis and Control of This Neglected Tropical Disease? *Plos Neglect Trop D* **8**, doi:ARTN e3349 10.1371/journal.pntd.0003349 (2014).

2 Schwede, A., Macleod, O. J. S., MacGregor, P. & Carrington, M. How Does the VSG Coat of Bloodstream Form African Trypanosomes Interact with External Proteins? *Plos Pathogens* **11**, doi:ARTN e1005259 10.1371/journal.ppat.1005259 (2015).

3 Schwede, A. & Carrington, M. Bloodstream form trypanosome plasma membrane proteins: antigenic variation and invariant antigens. *Parasitology* **137**, 2029-2039, doi:10.1017/S0031182009992034 (2010).

4 Macleod, O. J. S. *et al.* Invariant surface glycoprotein 65 of Trypanosoma brucei is a complement C3 receptor. *Nat Commun* **13**, 5085, doi:10.1038/s41467-022-32728-9 (2022).

5 Macleod, O. J. S. *et al.* A receptor for the complement regulator factor H increases transmission of trypanosomes to tsetse flies. *Nat Commun* **11**, doi:ARTN 1326 10.1038/s41467-020-15125-y (2020).

6 Gros, P., Milder, F. J. & Janssen, B. J. Complement driven by conformational changes. *Nat Rev Immunol* **8**, 48-58, doi:10.1038/nri2231 (2008).

7 Zipfel, P. F., Hallstrom, T. & Riesbeck, K. Human complement control and complement evasion by pathogenic microbes--tipping the balance. *Mol Immunol* **56**, 152-160, doi:10.1016/j.molimm.2013.05.222 (2013).

8 Ricklin, D., Reis, E. S., Mastellos, D. C., Gros, P. & Lambris, J. D. Complement component C3-The "Swiss Army Knife" of innate immunity and host defense. *Immunol Rev* **274**, 33-58, doi:10.1111/imr.12500 (2016).

9 Nilsson, B. & Nilsson Ekdahl, K. The tick-over theory revisited: is C3 a contact-activated protein? *Immunobiology* **217**, 1106-1110, doi:10.1016/j.imbio.2012.07.008 (2012).
10 Rooijakkers, S. H. *et al.* Structural and functional implications of the alternative complement pathway C3 convertase stabilized by a staphylococcal inhibitor. *Nat Immunol* **10**, 721-727, doi:10.1038/ni.1756 (2009).
11 Rosenthal, L. A., Sutterwala, F. S., Kehrli, M. E. & Mosser, D. M. Leishmania major-human macrophage interactions: cooperation between Mac-1 (CD11b/CD18) and complement receptor type 1 (CD35) in promastigote adhesion. *Infect Immun* **64**, 2206-2215, doi:10.1128/iai.64.6.2206-2215.1996 (1996).
12 Bradbury, L. E., Kansas, G. S., Levy, S., Evans, R. L. & Tedder, T. F. The CD19/CD21 signal transducing complex of human B lymphocytes includes the target of antiproliferative antibody-1 and Leu-13 molecules. *J Immunol* **149**, 2841-2850 (1992).
13 Fischer, M. B. *et al.* Dependence of germinal center B cells on expression of CD21/CD35 for survival. *Science* **280**, 582-585, doi:10.1126/science.280.5363.582 (1998).
14 Croix, D. A. *et al.* Antibody response to a T-dependent antigen requires B cell expression of complement receptors. *J Exp Med* **183**, 1857-1864, doi:10.1084/jem.183.4.1857 (1996).
15 Erdei, A. *et al.* Non-identical twins: Different faces of CR3 and CR4 in myeloid and lymphoid cells of mice and men. *Semin Cell Dev Biol* **85**, 110-121, doi:10.1016/j.semcdb.2017.11.025 (2019).
16 Capron, M. *et al.* Functional role of the alpha-chain of complement receptor type 3 in human eosinophil-dependent antibody-mediated cytotoxicity against schistosomes. *J Immunol* **139**, 2059-2065 (1987).
17 Tegla, C. A. *et al.* Membrane attack by complement: the assembly and biology of terminal complement complexes. *Immunol Res* **51**, 45-60, doi:10.1007/s12026-011-8239-5 (2011).
18 Couves, E. C. *et al.* Structural basis for membrane attack complex inhibition by CD59. *Nat Commun* **14**, 890, doi:10.1038/s41467-023-36441-z (2023).
19 Lambris, J. D., Ricklin, D. & Geisbrecht, B. V. Complement evasion by human pathogens. *Nat Rev Microbiol* **6**, 132-142, doi:10.1038/nrmicro1824 (2008).
20 Hammel, M. *et al.* A structural basis for complement inhibition by Staphylococcus aureus. *Nat Immunol* **8**, 430-437, doi:10.1038/ni1450 (2007).
21 Ricklin, D., Ricklin-Lichtsteiner, S. K., Markiewski, M. M., Geisbrecht, B. V. & Lambris, J. D. Cutting edge: members of the Staphylococcus aureus extracellular fibrinogen-binding protein family inhibit the interaction of C3d with complement receptor 2. *J Immunol* **181**, 7463-7467, doi:10.4049/jimmunol.181.11.7463 (2008).
22 Isenman, D. E., Leung, E., Mackay, J. D., Bagby, S. & van den Elsen, J. M. Mutational analyses reveal that the staphylococcal immune evasion molecule Sbi and complement receptor 2 (CR2) share overlapping contact residues on C3d: implications for the controversy regarding the CR2/C3d cocrystal structure. *J Immunol* **184**, 1946-1955, doi:10.4049/jimmunol.0902919 (2010).
23 Forneris, F. *et al.* Structures of C3b in Complex with Factors B and D Give Insight into Complement Convertase Formation. *Science* **330**, 1816-1820, doi:10.1126/science.1195821 (2010).
24 Rooijakkers, S. H. M. *et al.* Structural and functional implications of the alternative complement pathway C3 convertase stabilized by a staphylococcal inhibitor. *Nat Immunol* **10**, 721-U772, doi:10.1038/ni.1756 (2009).
25 Clark, E. A. *et al.* A structural basis for Staphylococcal complement subversion: X-ray structure of the complement-binding domain of Staphylococcus aureus protein Sbi in complex with ligand C3d. *Mol Immunol* **48**, 452-462, doi:10.1016/j.molimm.2010.09.017 (2011).

26 Janssen, B. J., Christodoulidou, A., McCarthy, A., Lambris, J. D. & Gros, P. Structure of C3b reveals conformational changes that underlie complement activity. *Nature* **444**, 213-216, doi:10.1038/nature05172 (2006).
27 Jumper, J. *et al.* Highly accurate protein structure prediction with AlphaFold. *Nature* **596**, 583-589, doi:10.1038/s41586-021-03819-2 (2021).
28 Janssen, B. J. *et al.* Structures of complement component C3 provide insights into the function and evolution of immunity. *Nature* **437**, 505-511, doi:10.1038/nature04005 (2005).
29 Forneris, F. *et al.* Structures of C3b in complex with factors B and D give insight into complement convertase formation. *Science* **330**, 1816-1820, doi:10.1126/science.1195821 (2010).
30 Noris, M. & Remuzzi, G. Overview of complement activation and regulation. *Semin Nephrol* **33**, 479-492, doi:10.1016/j.semnephrol.2013.08.001 (2013).
31 Morgan, H. P. *et al.* Structural basis for engagement by complement factor H of C3b on a self surface. *Nat Struct Mol Biol* **18**, 463-470, doi:10.1038/nsmb.2018 (2011).
32 Wiesmann, C. *et al.* Structure of C3b in complex with CRIg gives insights into regulation of complement activation. *Nature* **444**, 217-220, doi:10.1038/nature05263 (2006).
33 Forneris, F. *et al.* Regulators of complement activity mediate inhibitory mechanisms through a common C3b-binding mode. *EMBO J* **35**, 1133-1149, doi:10.15252/embj.201593673 (2016).
34 van den Elsen, J. M. & Isenman, D. E. A crystal structure of the complex between human complement receptor 2 and its ligand C3d. *Science* **332**, 608-611, doi:10.1126/science.1201954 (2011).
35 Bajic, G., Yatime, L., Sim, R. B., Vorup-Jensen, T. & Andersen, G. R. Structural insight on the recognition of surface-bound opsonins by the integrin I domain of complement receptor 3. *Proc Natl Acad Sci U S A* **110**, 16426-16431, doi:10.1073/pnas.1311261110 (2013).
36 Caesar, J. *et al.* SIMPLE 3.0. Stream single-particle cryo-EM analysis in real time. *J Struct Biol X* **4**, 100040, doi:10.1016/j.yjsbx.2020.100040 (2020).
37 Punjani, A., Rubinstein, J. L., Fleet, D. J. & Brubaker, M. A. cryoSPARC: algorithms for rapid unsupervised cryo-EM structure determination. *Nat Methods* **14**, 290-296, doi:10.1038/nmeth.4169 (2017).
38 Bepler, T. *et al.* Positive-unlabeled convolutional neural networks for particle picking in cryo-electron micrographs. *Nat Methods* **16**, 1153-1160, doi:10.1038/s41592-019-0575-8 (2019).
39 Zivanov, J. *et al.* New tools for automated high-resolution cryo-EM structure determination in RELION-3. *Elife* **7**, doi:10.7554/eLife.42166 (2018).
40 Zivanov, J., Nakane, T. & Scheres, S. H. W. A Bayesian approach to beam-induced motion correction in cryo-EM single-particle analysis. *IUCrJ* **6**, 5-17, doi:10.1107/S205225251801463X (2019).
41 Pettersen, E. F. *et al.* UCSF ChimeraX: Structure visualization for researchers, educators, and developers. *Protein Sci* **30**, 70-82, doi:10.1002/pro.3943 (2021).
42 Croll, T. I. ISOLDE: a physically realistic environment for model building into low-resolution electron-density maps. *Acta Crystallogr D Struct Biol* **74**, 519-530, doi:10.1107/S2059798318002425 (2018).
43 Emsley, P., Lohkamp, B., Scott, W. G. & Cowtan, K. Features and development of Coot. *Acta Crystallogr D Biol Crystallogr* **66**, 486-501, doi:10.1107/S0907444910007493 (2010).
44 Schindelin, J. *et al.* Fiji: an open-source platform for biological-image analysis. *Nat Methods* **9**, 676-682, doi:10.1038/nmeth.2019 (2012).
45 Wang, S., Ma, J. Z. & Xu, J. B. AUCpreD: proteome-level protein disorder prediction by AUC-maximized deep convolutional neural fields. *Bioinformatics* **32**, 672-679, doi:10.1093/bioinformatics/btw446 (2016).

46 Williams, C. J. *et al.* MolProbity: More and better reference data for improved all-atom structure validation. *Protein Sci* **27**, 293-315, doi:10.1002/pro.3330 (2018).
47 Adams, P. D. *et al.* PHENIX: a comprehensive Python-based system for macromolecular structure solution. *Acta Crystallogr D Biol Crystallogr* **66**, 213-221, doi:10.1107/S0907444909052925 (2010).

Figures

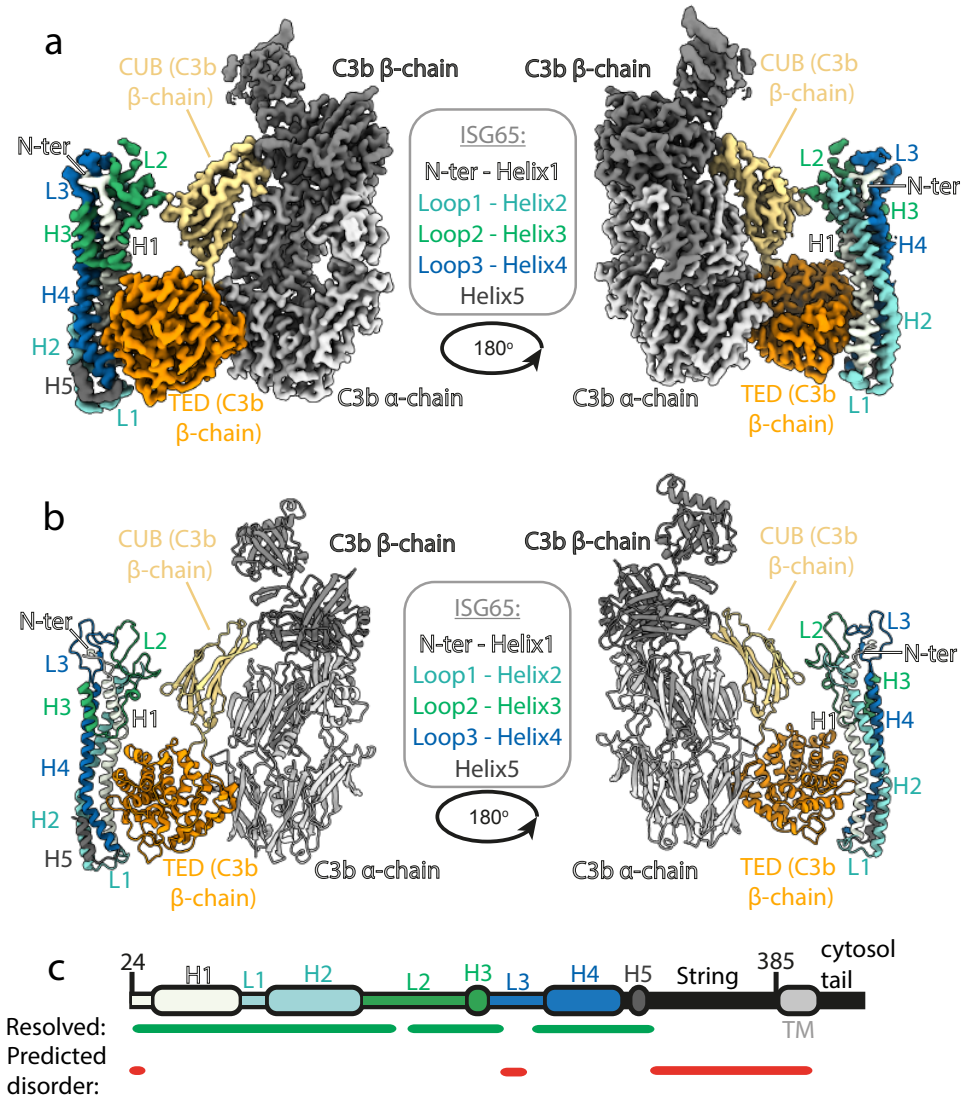

Figure 1: Structure of the complex between ISG65 and human C3b

a) Composite volume of locally refined regions determined using cryogenic electron microscopy for ISG65 bound to human C3b. ISG65 is coloured in different shades of blue and green, as indicated in the legend in the centre of the panel (loop1 and helix 2 are light blue, loop 2 and helix 3 are green and loop3 and helix 4 are dark blue). C3b is coloured in grey scale with the α-chain in light grey and the β-chain in dark grey. The TED domain is highlighted in orange and the CUB domain highlighted in yellow. **b)** Molecular model of the same complex with a colour scheme matching that of a). **c)** A schematic showing the features of ISG65, coloured as a). Regions resolved in the structure are indicated underneath the schematic using a green line and regions predicted to be disordered using AUCpreD[45] are shown by the red line.

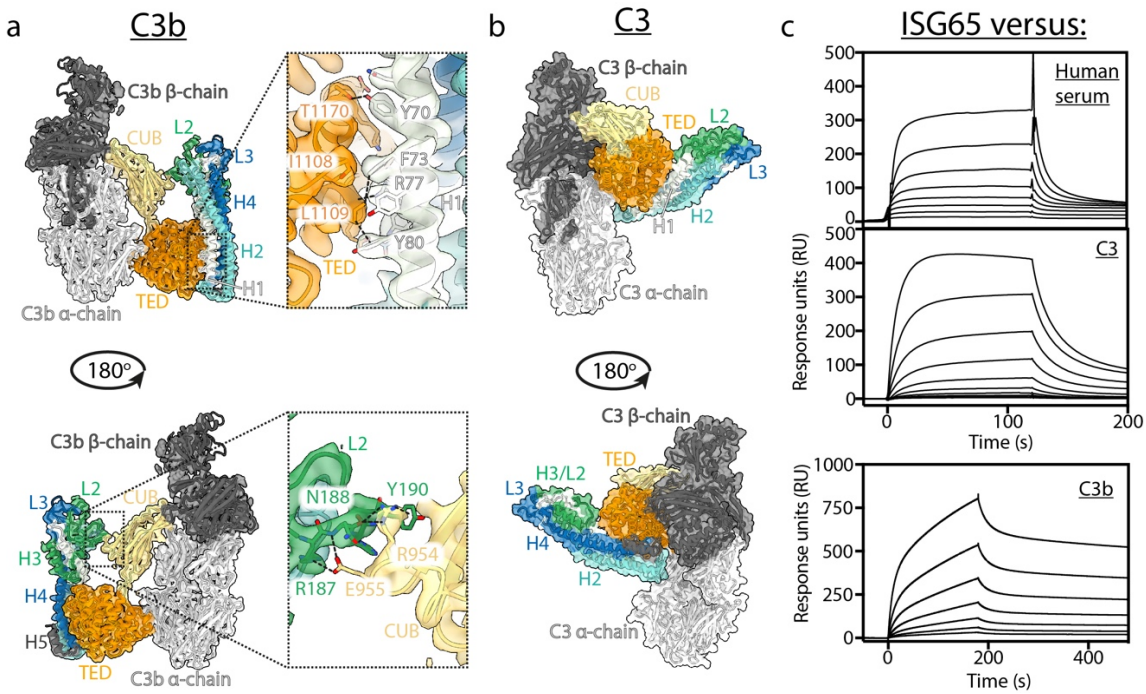

Figure 2: ISG65 forms two distinct interfaces with the TED and CUB domains of C3b

a) The ISG65-C3b model shown in transparent cryo-EM density. The top panel shows the interface between ISG65 and the TED domain (orange), with bottom panel showing the interface between loop L2 of ISG65 (green) and the CUB domain of C3b (yellow). In each case, the left-hand panel shows the intact structure, with a dotted box highlighting the region shown in an enlarged form in the right-hand panel. **b)** The ISG65 model superimposed onto a previously determined structure of C3 (PDB ID: 2A73)[28] via the TED domain of the ISG65-C3b model. This is shown as a ribbon within a transparent surface representation. ISG65 can bind to C3 via the TED domain, via the same interface as previously identified for ISG65-C3d[4]. **c**) Surface plasmon resonance data showing responses from the injection of human serum (two-fold dilutions from a concentration of 8 mg/mL), C3 (two-fold dilutions from a concentration of 625 nM) and C3b (two-fold dilutions from a concentration of 500 nM, data previously shown[4]) over a flow cell conjugated with ISG65.

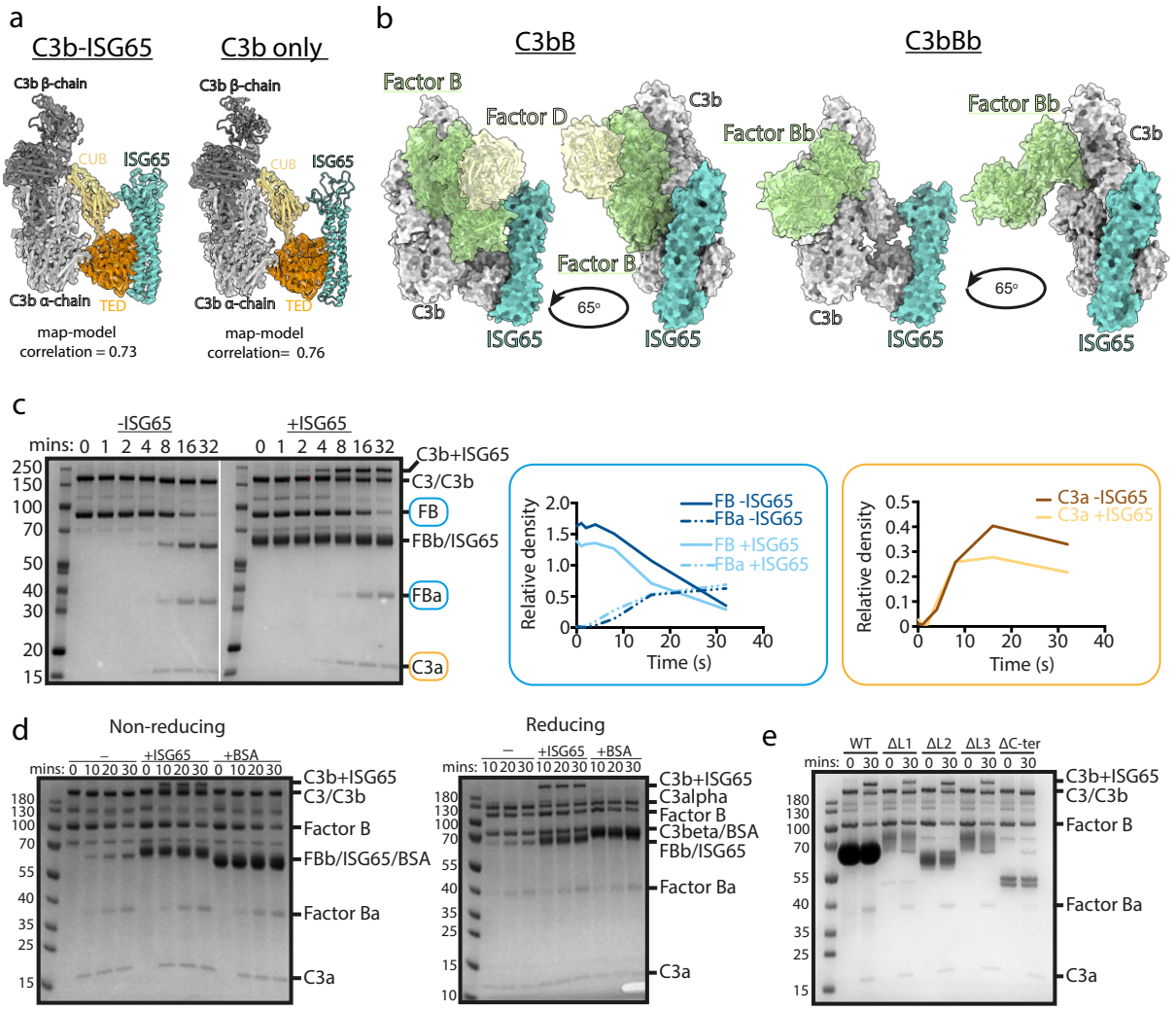

Figure 3: ISG65 does not block the formation of the C3 convertase

a) The structure of the ISG65-C3b complex docked into the electron microscopy-derived volumes obtained for the ISG65-C3b complex (left) and C3b alone (right). **b)** Composite models obtained by docking the C3b-ISG65 structure onto those of C3b bound to factors B and D (PDB ID: 2XWJ)[29] or factor Bb (6RUR)[10]. **c)** An assay for C3 convertase formation in which C3b and factor D were each added at concentrations of 12 nM and C3 and factor B at concentrations of 600 nM. Samples were taken at different time points and were analysed by SDS-PAGE analysis with Coomassie straining. This was done in the absence (left-hand gel) and presence (right-hand gel) of 2 μM ISG65. The graphs show quantification by densitometry for factors B, Ba and C3a to assess convertase function. **d)** An equivalent assay to that shown in c), conducted in the absence of non-complement protein (left), or the presence of 2 μM ISG65 (central) or 2 μM BSA (right). The left-hand gel was run in non-reducing conditions while the right-hand gel was run in reducing conditions. **e).** An equivalent assay to that shown in c), conducted in presence of 2 μM ISG65 or of ISG65 variants lacking loop 1 (ΔL1), loop 2 (ΔL1), loop 3 (ΔL1) or the extended disordered C-terminal region (ΔC).

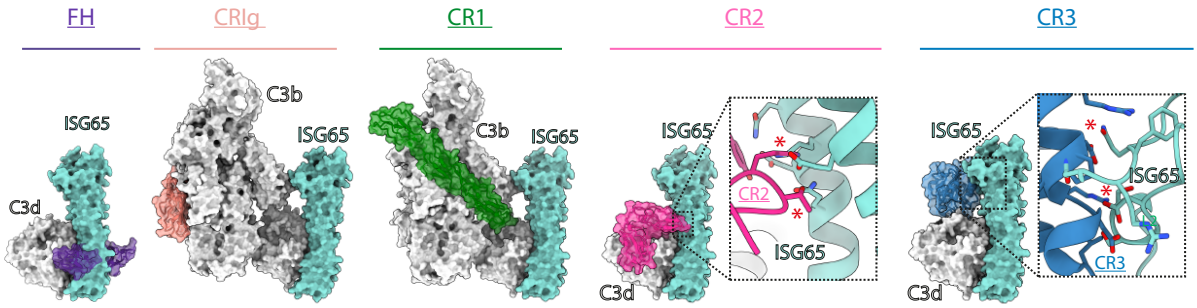

Figure 4: ISG65 overlaps the binding sites for complement receptors 2 and 3

Composite models obtained by docking the C3b-ISG65 structure onto those of C3b/d bound to factor H CCP19-20 (3OXU)[31], CRIg (2ICF)[32], CR1 CCP15-17 (5FO9)[33], CR2 SCR1-2 (3OED)[34] and CR3 I-domain (4M76)[35]. C3b/d is shown in a solid light grey surface, ISG65 is shown in a solid turquoise surface, and complement regulators are shown in transparent surface with ribbon in various colours.

Supplementary Figures

Supplementary Figure 1: Workflow of Cryo-EM data processing

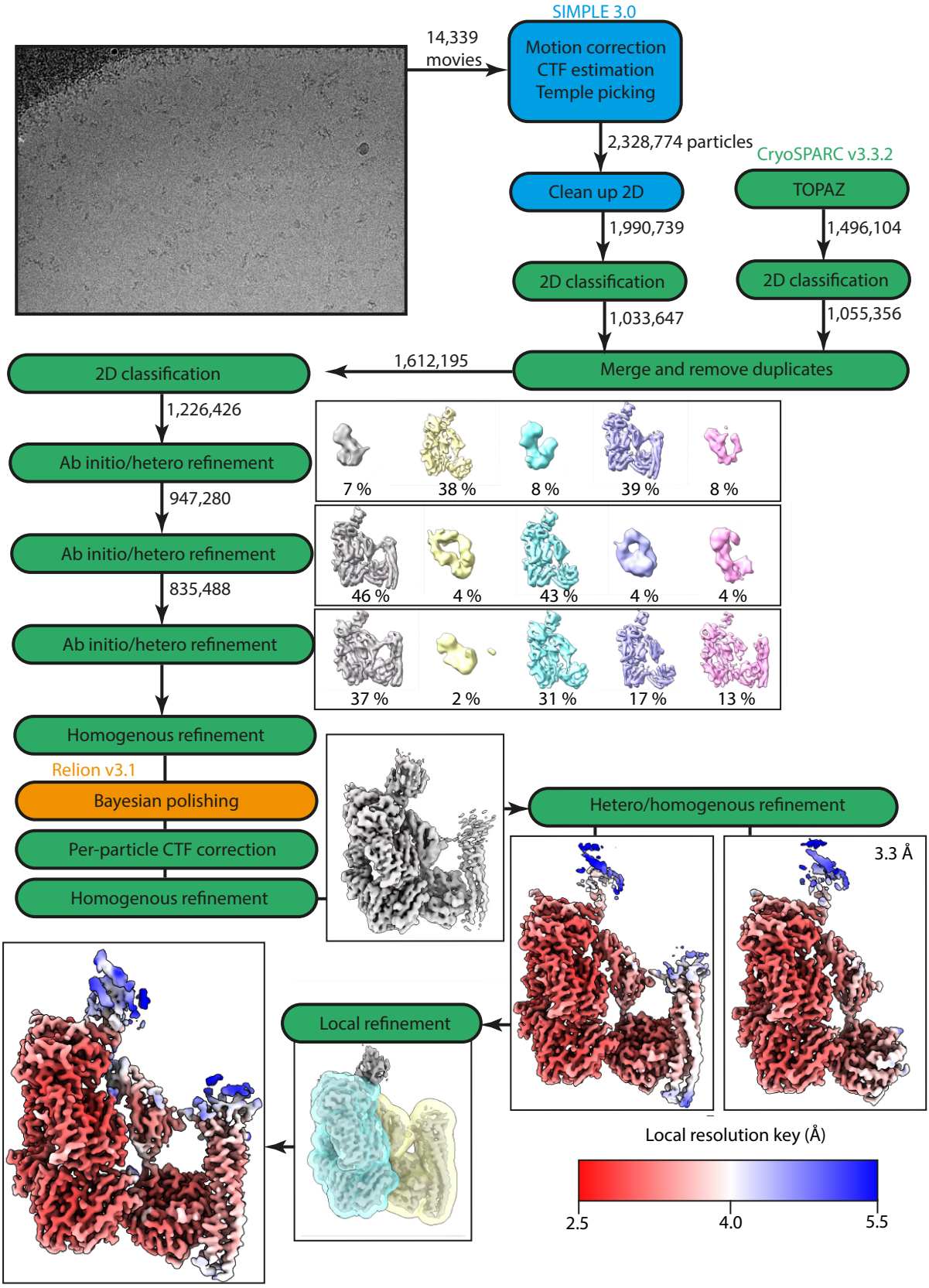

Supplementary Table 1: Cryo-EM data collection and model building statistics.

	EMDB-17209 PDB-8OVB	EMDB-17219	EMDB-17220	EMDB-17221
	Composite map	**Local CUB-TED-ISG65 refinement**	**Local C3c refinement**	**C3b only**
Data collection				
Microscope		Titan Krios		
Detector		Gatan K3 with 20 eV Energy Filter		
Voltage (kV)		300		
Pixel size (Å)		0.832		
Dose rate (e^{-}/Å^2)		49		
Total exposure (s)		3.03		
Frames per movie		40		
Defocus range (µm)		-1.0 to -3.0		
EM data processing				
Number of micrographs		14,339	14,339	14,339
Box size (pixels)		336	336	336
Initial particle number		3,824,878	3,824,878	3,824,878
Cleaned particle number		835,488	835,488	835,488
Final particle number		481,606	481,606	382,161
Symmetry		C1	C1	C1
Map resolution (Å)		3.4	3.2	3.4
FSC threshold		0.143	0.143	0.143
Map resolution range (Å)		2.9-8.1	2.8-7.2	2.8-13.6
FSC threshold		0.5	0.5	
Map postprocessing		DeepEMhancer	DeepEMhancer	DeepEMhancer
Map combination method	ChimeraX			
Model refinement				
Initial model used	AlphaFold2 (ISG65), 5FO7 (C3b)			
Model composition [a]				
Chains	3			
Protein residues	1826			
Non-hydrogen protein atoms	14429			
Root mean square Z-score[a]				
Bond lengths	0.59			
Bond angles	0.93			
Validation[b]				
Molprobity score	1.17			
Clash score	0.17			
Rotamers favoured (%)	92.4			
Rotamer outliers (%)	2.76			
Model vs. Map[c]				
FSC (0.5) (Å)	3.6			
CC (mask)	0.73			
Ramachandran plot[b]				
Favoured (%)	96.1			
Outliers (%)	0			

[a] Statistics calculated using the PDB validation server
[b] Statistics calculated using Molprobity[46]
[c] Statistics calculated using PHENIX[47]

Supplementary Table 2: Kinetic parameters of C3 and C3b binding to ISG65 measured by surface plasmon resonance.

	k_{a1} ($M^{-1}s^{-1}$)	k_{d1} (s^{-1})	k_{a2} (s^{-1})	k_{d2} (s^{-1})	K_D (nM)	Chi^2 (RU^2)
C3	9.7×10^4	0.03	-	-	280	189
C3b[4]	7×10^4	0.05	0.01	7×10^4	40	59